Poly(methyl methacrylate)/Montmorillonite Nanocomposites Prepared with a Novel Reactive Phosphorus–Nitrogen-Containing Monomer of *N*-(2-(5,5-dimethyl-1,3,2-dioxaphosphinyl-2-ylamino)ethyl)-Acrylamide and Its Thermal and Flame Retardant Properties

Guobo Huang,[1] Xu Wang,[2] Zhengdong Fei,[2] Huading Liang,[1] Yuyuan Ye[1]

[1]*School of Pharmaceutical and Chemical Engineering, Taizhou University, Linhai 317000, People's Republic of China*
[2]*College of Chemical Engineering and Materials, Zhejiang University of Technology, Hangzhou 310014, People's Republic of China*

Received 27 June 2011; accepted 10 September 2011
DOI 10.1002/app.35618
Published online 11 December 2011 in Wiley Online Library (wileyonlinelibrary.com).

ABSTRACT: A novel reactive phosphorus–nitrogen-containing monomer, *N*-(2-(5,5-dimethyl-1,3,2-dioxaphosphinyl-2-ylamino)ethyl)-acrylamide (DPEAA), was synthesize and characterized. Flame retardant poly(methyl methacrylate)/organic-modified montmorillonite (PMMA-DPEAA/OMMT) nanocomposites were prepared by *in situ* polymerization by incorporating methyl methacrylate, DPEAA, and OMMT. The results from X-ray diffraction and transmission electron microscopy (TEM) showed that exfoliated PMMA-DPEAA/OMMT nanocomposites were formed. Thermal stability and flammability properties were investigated by thermogravimetric analysis, cone calorimeter, and limiting oxygen index (LOI) tests. The synergistic effect of DPEAA and montmorillonite improved thermal stability and reduced significantly the flammability [including peak heat release rates (PHRR), total heat release, average mass loss rate, etc.]. The PHRR of PMMA-DPEAA/OMMT was reduced by about 40% compared with pure PMMA. The LOI value of PMMA-DPEAA/OMMT reached 27.3%. The morphology and composition of residues generated after cone calorimeter tests were investigated by scanning electronic microscopy (SEM), TEM, and energy dispersive X-ray (EDX). The SEM and TEM images showed that a compact, dense, and uniform intumescent char was formed for PMMA-DPEAA/OMMT nanocomposites after combustion. The results of EDX confirmed that the carbon content of the char for PMMA-DPEAA/OMMT nanocomposites increased obviously by the synergistic effect of DPEAA and montmorillonite. J Appl Polym Sci 124: 5037–5045, 2012

Key words: clay; flame retardant; nanocomposites

INTRODUCTION

Poly(methyl methacrylate) (PMMA) is a typical transparent amorphous polymer and has been widely used in a wide range of fields with several desirable properties such as good flexibility, high strength, and excellent dimension stability. However, PMMA is very flammable and cannot satisfy some applications which require high flame retardancy. Incorporating a chemically reactive flame retardant monomer into the polymer chain is one of the most efficient methods of improving the flame retardancy of polymer. Some phosphorus-containing components have already been used in the synthesis of several flame retardant step-reaction polymers, e.g., polyesters,[1,2] polyurethanes,[3] and epoxy resins.[4–6] However, phosphorus–nitrogen-containing components used in the synthesis of chain-reaction polymers are much less well developed.[7] In this article, a novel reactive phosphorus–nitrogen-containing monomer, *N*-(2-(5,5-dimethyl-1,3,2-dioxaphosphinyl-2-ylamino)ethyl)-acrylamide (DPEAA), was synthesized and applied to prepare flame retardancy PMMA.

Polymer-layered silicate nanocomposites (PLSN) consisting of continuous polymer matrix reinforced by a few weight percent of intercalated or exfoliated layered silicates have drawn more and more attention in recent years due to their unique materials properties.[8–17] As an important member of such nanocomposites, PLSN exhibit enhanced thermal stability and flame retardancy, reduced gas permeability, and improved physical performance and barrier properties. PLSN exhibit enhanced thermal stability and flame retardancy, reduced gas permeability, and improved physical

Correspondence to: G. Huang (huangguobo@tzc.eud.cn).
Contract grant sponsor: Zhejiang Provincial Natural Science Foundation of China; contract grant number: Y4110026.
Contract grant sponsor: Opening Foundation of Zhejiang Provincial Top Key Discipline; contract grant number: 20110913.

performance and barrier properties. Previous researches of the flame retardant properties of PLSN mainly demonstrate a significant decrease in the heat release rate, a change in the char structure, and a decrease in the mass loss rate during combustion in a cone calorimeter.[18–26] In fact, most of PLSN usually do not extinguish and burn slowly until most of the fuel has been burnt. To further improve flame retarding performance of PLSN, intumescent flame retardant (IFR), as environmentally friendly halogen-free products, is widely applied in the preparation of flame retardant PLSN.[27–30] The IFR can generate a swollen multicellular thermally stable char during burning which insulates the underlying material from the flame action. Previous study showed that the addition of montmorillonite into PMMA improved flame retardancy and reduced the heat release rate.[31–33] However, little work has been done concerning the synergistic effect between IFR and the clay mineral in PMMA nanocomposites.

In this article, flame retardant PMMA/montmorillonite nanocomposites were prepared by *in situ* polymerization by incorporating methyl methacrylate (MMA), DPEAA, and OMMT. The thermal property and flammability of PMMA/montmorillonite nanocomposites were investigated by thermogravimetric analysis (TGA) and cone calorimeter test. The char residue after combustion was also examined by scanning electronic microscopy (SEM), *transmission electron microscopy* (TEM), and energy dispersive X-ray (EDX). It is anticipated that the combination of montmorillonite and IFR DPEAA could improve the thermal stability and flame retardant of the nanocomposites.

EXPERIMENTAL

Materials

Neopentyl glycol, acryloyl chloride, MMA, and benzoyl peroxide (BPO) chemically pure (CP) were purchased from Sinopharm Chemical Reagent Co. (Shanghai, China). Phosphoryl trichloride and ethylenediamine (CP) were supplied by Shanghai Chemical Reagent Co. (Shanghai, China). Pristine sodium montmorillonite (Na-MMT), with a cation exchange capacity of ~120 mequiv./100 g, was mined at An'ji, Zhejiang, China and was supplied by Anji Yu Hong Clay Chemical Co. (Zhejiang, China). The OMMT was prepared by ion exchange of Na-MMT and hexadecyl trimethyl ammonium bromide in aqueous solution. 2,2-Dimethyl-1,3-propanediol phosphoryl chloride (DPPC) and [1] *N*-(5,5-dimethyl-1,3,2-dioxaphosphinyl-2-yl)ethane-1,2-diamine (DPEA) were prepared according to the published procedure (Scheme 1).[34,35]

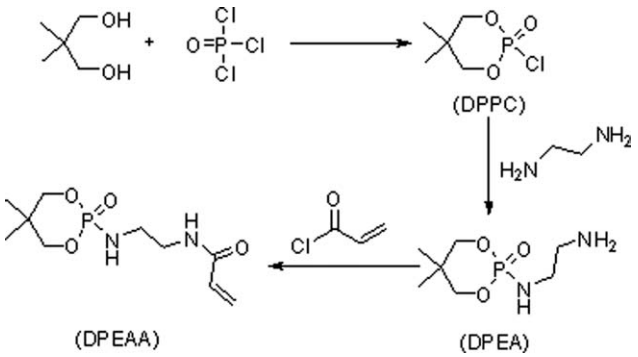

Scheme 1 Synthesis of nitrogen- and phosphorus-containing monomer of DPEAA.

Synthesis of DPEAA

DPEA (0.10 mol, 20.8 g), acryloyl chloride (0.10 mol, 9.0 g), triethylamine (0.20 mol, 20.2 g), and 50 mL dried trichloromethane were mixed in a glass flask. The reaction was completed after 6 h at 45°C. The raw product was filtered and purified with methyl alcohol. The purified product (DPEAA) was a white solid (yield: 74%). Fourier-transform infrared (FT-IR; KBr, cm^{-1}): 3190, 1728, 1478, 1269, 1224, 1068, and 1007. ^1H NMR (CCl_3D, δ): 7.27 (m, 1H), 6.30–6.27 (m, 1H), 6.18–6.15 (m, 1H), 5.62–5.60 (m, 1H), 4.22–4.18 (m, 2H), 3.87–3.82 (m, 2H), 3.46–3.45 (m, 2H), 3.16–3.12 (m, 2H), 1.16 (s, 3H), and 0.93 (s, 3H). ^{13}C NMR (CCl_3D, δ): 166.19, 131.24, 125.71, 77.29, 76.78, 41.01, 31.81, 21.69, and 20.82. High-resolution mass spectrometry (HRMS) (ESI): $C_{10}H_{19}N_2O_4P$ calcd mass (M+H) 263.1161, found 263.1158.

Preparation of PMMA-DPEAA

A copolymer of MMA and DPEAA (PMMA-DPEAA) was prepared as follows: in a 4-neck round-bottom flask equipped with inlets for refrigeration, mechanical stirring, and nitrogen, kept in an oil bath at 90°C, 90 g of MMA, 10 g of DPEAA, and 0.5 g of BPO previously dissolved, was added. This solution was stirred mechanically at 90°C for 30 min and then inserted into a mold and kept at 80°C for 48 h to complete the polymerization process. Finally, the PMMA-DPEAA was kept for 6 h at 120°C to be sure that the entire prepolymer fraction has been converted. The copolymer modified by 5 wt % and 10 wt % DPEAA is denoted by PMMA-DPEAA5 and PMMA-DPEAA10, respectively.

Preparation of PMMA-DPEAA/OMMT nanocomposites

PMMA-DPEAA/OMMT nanocomposites were prepared as follows: first, an appropriate amount of OMMT (5 g) was introduced into the matrix of 85.5 g of MMA and 9.5 g of DPEAA monomers under

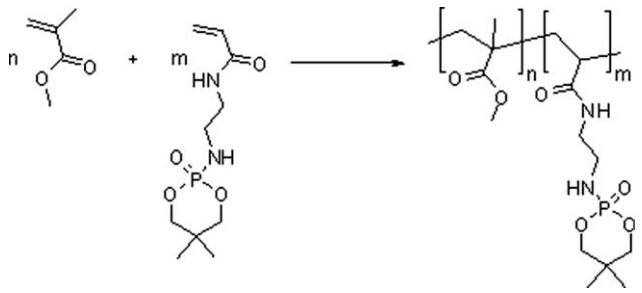

Scheme 2 Synthesis of PMMA-DPEAA.

magnetic stirring for 12 h at room temperature. On addition of BPO (0.5 g), this solution then was stirred mechanically at 90°C for 30 min and inserted into a mold and kept at 80°C for 48 h to complete the polymerization process. Finally, the PMMA-DPEAA/OMMT nanocomposites were then obtained by keeping for 6 h at 120°C. PMMA filled with 5 wt % OMMT is denoted by PMMA/OMMT.

Characterization and measurement

The samples of PMMA and PMMA-DPEAA for FT-IR were extracted with acetone for 24 h in a Soxhlet extraction apparatus. The FT-IR spectra of compound DPEAA and PMMA-DPEAA (30 wt % DPEAA) dispersed in potassium bromide discs were recorded with Nicolet (model 5700 FT-IR) spectrophotometer, scanning range 400–4000 cm^{-1}. ^1H NMR spectra were recorded by a Bruker Avance III (500 MHz) spectrometer in CCl_3D, using tetramethylsilane as an internal standard. HRMS was performed with a Therm LCQ TM Deca XP plus mass spectrometer coupled to a Waters 2695 liquid chromatograph. Differential scanning calorimeter (DSC) measurements were performed under dry nitrogen by using a DSC 200F3 DSC thermal analyzer. All samples of DSC were measured from room temperature to 300°C at a heating rate of 10°C/min with a nitrogen flow of 50 mL/min. X-ray diffraction (XRD) patterns were obtained in a Thermo ARL X-TRA diffractometer using a CuK-α radiation generator with an intensity of 40 mA and a voltage of 40 kV. The diffraction patterns were collected within the 2θ range of 2–12° using a scanning rate of 0.6°/min. The nanocomposites were examined by TEM using a JEM-1230 TEM operating at 80 kV. TGA was carried out on a Q600SDT thermogravimetric analyzer. Sample weights were the range of 12–15 mg. All TGA samples were measured from 30°C to 600°C at a heating rate of 10°C/min with a nitrogen flow of 100 mL/min. The flame retardant characteristics of PMMA-DPEAA, and its nanocomposites were tested using a cone calorimeter (ISQ5660) with a heat flux of 35 kW/m^2 using a cone radiator. All samples with the dimensions of 10 cm × 10 cm × 3 mm plates were placed in aluminum foil, and then put in a box with the same dimension in the horizontal direction. The limiting oxygen index (LOI) was measured with sheet dimensions of 120 × 6.5 × 3 mm^3 according to GB/T 2406-93. The cone data reported here are an average of three replicated measurements. Char residue was examined by using a Hitachi S-4800(II) SEM. EDX measurements were conducted on a Noran Vantage-ESI EDX micro analyzer equipped in the SEM.

RESULTS AND DISCUSSION

Preparation and characterization of PMMA-DPEAA

As shown in Scheme 2, flame retardant PMMA-DPEAA was prepared by the free radical polymerization of MMA and DPEAA. FT-IR spectra of DPEAA, PMMA, and PMMA-DPEAA were presented in Figure 1. In the FT-IR spectrum of DPEAA, the absorption peaks at 3207 cm^{-1} (N–H), 1569 cm^{-1} (C=C), 1220 cm^{-1} (P–O), 1060 cm^{-1} and 1009 cm^{-1} (P–O–C), and 948 cm^{-1} (P–N) were found. Compared with the FT-IR spectrum of DPEAA, the characteristic peaks of carbon–carbon double bond in DPEAA disappeared from the spectrum of PMMA-DPEAA, demonstrating that the carbon–carbon double bond on DPEAA had reacted with MMA by free radical polymerization. PMMA-DPEAA showed that several new bands appeared relative to pure PMMA. The band at 3198 cm^{-1} and 1224 cm^{-1} was corresponding to the stretching band of N–H and P–O, respectively, and the band at 1058 cm^{-1} and 1008 cm^{-1} was interpreted to the stretching band of P–O.[35] What mentioned above indicated that a copolymer of MMA and DPEAA had produced by free radical polymerization.

PMMA-DPEAA was characterized by ^1H NMR as shown in Figure 2. In the ^1H NMR spectrum of PMMA-DPEAA, the resonance signals occurring at

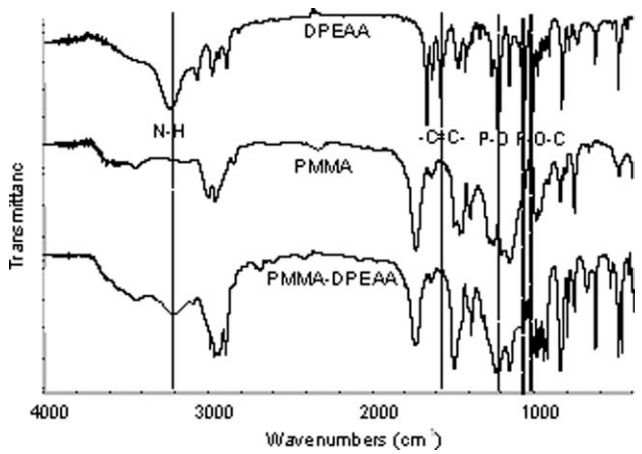

Figure 1 FT-IR spectra of DPEAA, PMMA, and PMMA-DPEAA.

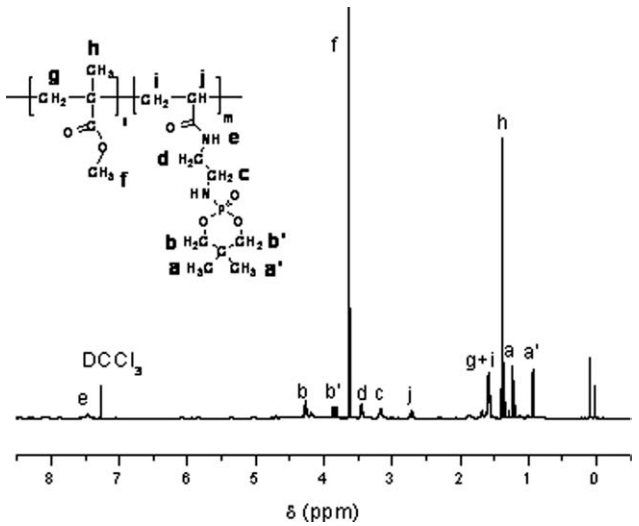

Figure 2 ^{1}H NMR spectrum of PMMA-DPEAA.

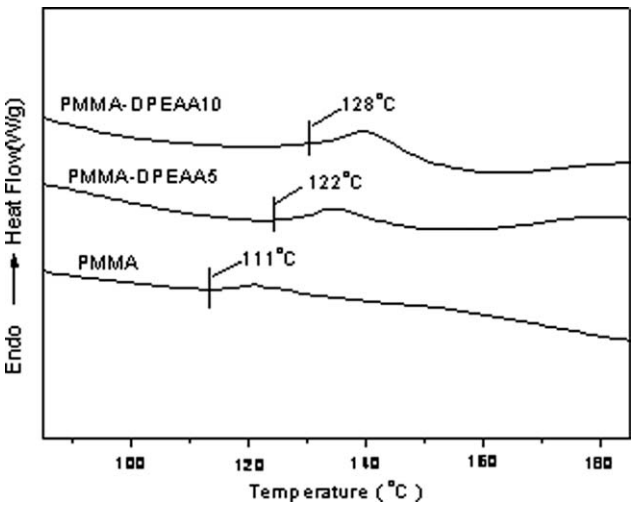

Figure 3 DSC thermograms of PMMA, PMMA-DPEAA5, and PMMA-DPEAA10.

1.11, 0.94 (a, a′), 4.25, 3.88 (b, b′) and 3.08, 3.45 (c, d) ppm were remarkably ascribed to methyl, methylene linked to phosphoric acid ester group, and the middle methylene of DPEAA, respectively.[34,35] The signals at 3.63 (f) and 1.32 (h) ppm were assigned to the methyl of MMA. Particularly, the signals at 1.60–1.85 ppm (g, i) were caused by the methylene and methenyl groups of PMMA-DPEAA with different combinations of DPEAA and MMA. The appearances of these peaks indicated the random sequences of the chain of PMMA-DPEAA.

PMMA, PMMA-DPEAA5 and PMMA-DPEAA10 were measured by a DSC, and their glass transition temperature (T_g) was compared in Figure 3. As shown in Figure 3, only one single glass transition could be detected during heating, proving that the copolymer PMMA-DPEAA was random, which agrees with the ^{1}H NMR results that no obvious microphase separation occurs. The T_g of the PMMA-DPEAA10 sample was 17°C higher than that of pure PMMA. The monomer of DPEAA with bulky side groups might restrict the chain mobility of PMMA, which led to the increment of the T_g of PMMA-DPEAA. In addition, the T_g of PMMA-DPEAA increased with the increment of the DPEAA content.

Morphology of PMMA-DPEAA/OMMT nanocomposites

Figure 4 provided that the XRD curves of OMMT, PMMA/OMMT, and PMMA-DPEAA/OMMT. A diffraction peak around $2\theta = 4.48°$ was displayed by OMMT, equaling a d spacing of 1.90 nm for the layered silicates in OMMT. PMMA/OMMT showed a basal spacing of 2.98 nm. The increased spacing indicated that some PMMA molecular chains were intercalated. However, the characteristic (001) reflection of the layered silicates in the PMMA-DPEAA nanocomposites completely disappeared, indicating exfoliated silicate layers were dispersed in the PMMA-DPEAA matrix by *in situ* polymerization.

Figure 5 showed the TEM photomicrographs of PMMA/OMMT and PMMA-DPEAA/OMMT samples. From the TEM image of PMMA/OMMT, the clay mineral layers consisted of multilayered stacks and intercalated or exfoliated silicate layers can be observed. The TEM image of PMMA-DPEAA/OMMT sample revealed that most of the clay mineral layers lost their stacking structure and were dispersed disorderly in the PMMA-DPEAA matrix, which indicated that the clay mineral layers were delaminated. These results further supported by the XRD analysis results for the formation of the exfoliated nanocomposites.

Thermal properties

Figure 6 showed the TGA thermograms of PMMA, PMMA/OMMT, PMMA-DPEAA, and PMMA-

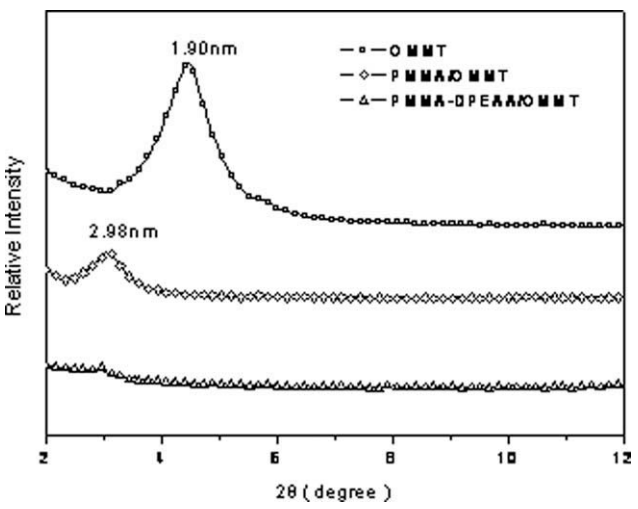

Figure 4 X-ray diffraction patterns of OMMT, PMMA/OMMT, and PMMA-DPEAA/OMMT.

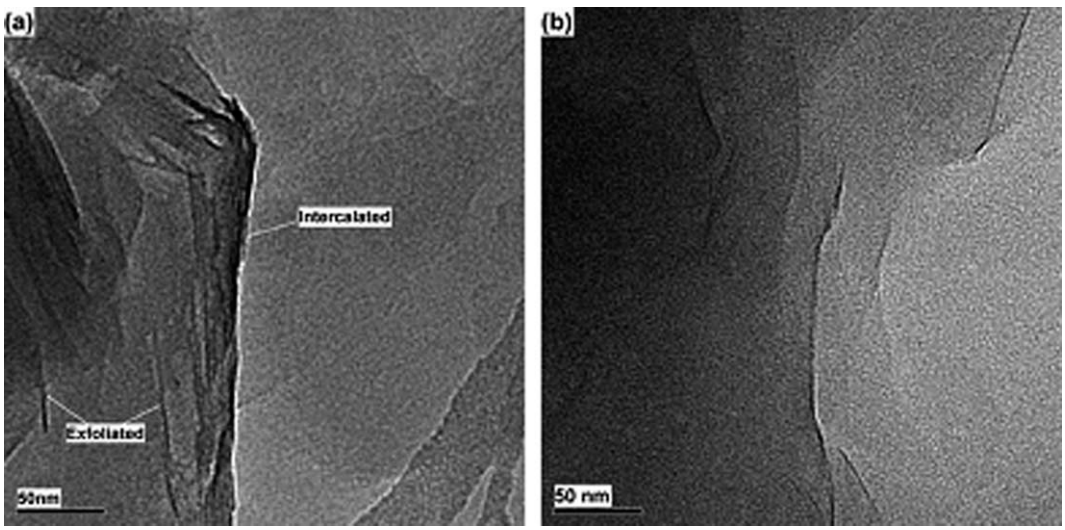

Figure 5 TEM images of (a) PMMA/OMMT and (b) PMMA-DPEAA/OMMT.

DPEAA/OMMT. The corresponding TGA data were presented in Table I. The temperature in which the weight loss is 5 wt % is defined as the initial decomposition temperature, which is denoted as T_{inital}. Pure PMMA decomposed at 269°C, leaving negligible char at 500°C. $T_{initial}$ of PMMA/OMMT was 2°C lower than pure PMMA due to the decomposition of the organic modifier. $T_{initial}$ of PMMA-DPEAA10 was 19°C higher than PMMA, and the $T_{initial}$ of PMMA-DPEAA was increased with the increment of the DPEAA content, which indicated that DPEAA had a significant effect on the thermal stability of PMMA. On the basis of Figure 6 and Table I, T_{inital} of PMMA-DPEAA/OMMT was higher than that of PMMA/OMMT and PMMA-DPEAA10, and the final char for PMMA-DPEAA/OMMT was 4 wt % higher than PMMA-DPEAA10, which indicated that the synergistic effect of DPEAA and montmorillonite significantly improved the thermal properties of PMMA.

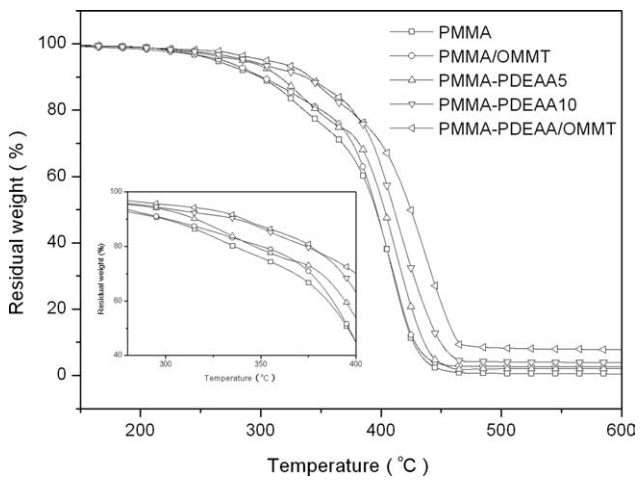

Figure 6 TGA curves for PMMA, PMMA/OMMT, PMMA-DPEAA, and PMMA-DPEAA/OMMT.

Flame retardant properties

Figure 7 showed that the heat release rate of PMMA, PMMA/OMMT, PMMA-DPEAA5, PMMA-DPEAA10, and PMMA-DPEAA/OMMT at 35 kW/m^2. The corresponding cone calorimetry and LOI data were shown in Table II. In comparison to pure PMMA, the peak heat release rates (PHRR) of PMMA/OMMT was 20% lower even though the total heat release (THR), and average mass loss rate (AMLR) remained almost same. The time of ignition (t_{ign}) of PMMA/OMMT was 5 s higher than that of pure PMMA, and the LOI value of PMMA/OMMT sample increased to 22.6%. Previous study also showed that the addition of OMMT reduced the flammability of PMMA.[31–33] For PMMA-DPEAA *copolymers*, both the PHRR AHRR and AMLR were reduced with the addition of DPEAA. The PHRR of PMMA-DPEAA5 and PMMA-DPEAA10 was reduced by 22% and 26% relative to pure PMMA. The THR was reduced by 12% and 15% for PMMA-DPEAA5 and PMMA-DPEAA10; the t_{ign} of PMMA-DPEAA blends was longer than that of pure PMMA. In addition, the LOI value of PMMA-DPEAA5 and PMMA-DPEAA10 was 23.7% and

TABLE I
Data of TGA Thermograms for Various Samples at a Heating Rate of 10°C/min in N_2

Sample	$T_{initial}$ (°C)	Char residue (%) 400°C	500°C	600°C
PMMA	269	43.6	0.7	0.5
PMMA/OMMT	267	43.9	2.7	2.6
PMMA-DPEAA5	281	48.4	2.1	2.1
PMMA-DPEAA10	288	60.5	4.1	3.9
PMMA-DPEAA/OMMT	292	63.0	8.1	7.7

$T_{initial}$, initial degradation temperature (temperature at 5 wt % loss).

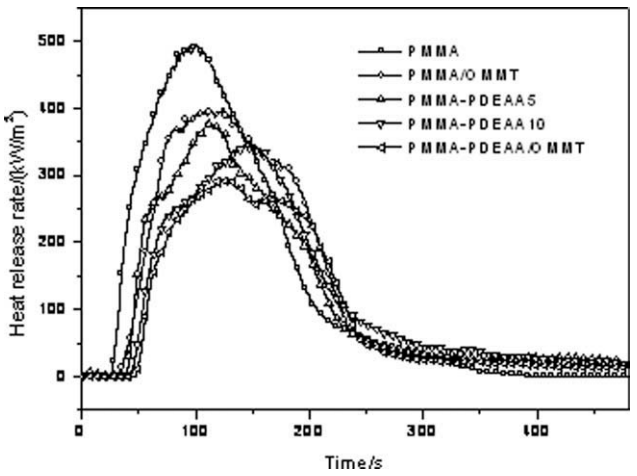

Figure 7 Heat release rate of PMMA, PMMA/OMMT, PMMA-DPEAA5, PMMA-DPEAA10, and PMMA-DPEAA/OMMT at 35 kW/m^2.

25.1%, respectively. These indicated that the phosphorus–nitrogen-containing monomer DPEAA improved significantly the flame retardant properties of PMMA. Compared with pure PMMA, the PHRR of PMMA-DPEAA/OMMT was reduced by about 40%. For PMMA-DPEAA/OMMT, t_{ign} was longer than that of those of PMMA/OMMT and PMMA-DPEAA10. Meanwhile, the values of PHRR, THR and AMLR of PMMA-DPEAA/OMMT were lower than those of PMMA/OMMT and PMMA-DPEAA10. The LOI value of PMMA-DPEAA/OMMT reached 27.3% and was higher than those of PMMA/OMMT and PMMA-DPEAA10. The improvement of flame retardancy of PMMA-DPEAA/OMMT indicated the synergistic effect between montmorillonite and DPEAA. The similar results were obtained for exfoliated ABS/MMT and PA6/MMT nanocomposites with phosphorus–nitrogen-containing flame retardant additive.[36,37]

Figure 8 showed the digital photos for the residues of PMMA, PMMA/OMMT, PMMA-DPEAA10, and PMMA-DPEAA/OMMT samples after cone calorimeter tests. The digital photos demonstrated that the pure PMMA left almost no residue at the end of combustion. The char of PMMA/OMMT was thin and discrete. For the PMMA-DPEAA10 sample, the swollen char was observed. For the PMMA-DPEAA/OMMT sample, the char was more rigid, compact, and uniform.

The morphologies of the char obtained after cone calorimeter test were examined by SEM, which were shown in Figure 9. A lot of clay mineral layers joined each other and formed a barrier in the residue of PMMA/OMMT. For the char of PMMA-DPEAA10 sample, intumescent carbonaceous structures were observed clearly. Residue of PMMA-DPEAA/OMMT showed that many clay mineral layers were dispersed uniformly on the char surface and formed a compact and dense barrier, which could form a better protective shields, and inhibit more effectively the transmission and diffusion of heat more effectively when exposed to flame or heat source.

TEM images of the residues after combustion were shown in Figure 10. The TEM image of the residues of PMMA/OMMT revealed that most of the clay mineral layers were stacked on top of each other after combustion. However, it was seen clearly that the highly exfoliated clay mineral layers were randomly dispersed in the char from the TEM image of the residues of PMMA-DPEAA/OMMT, which indicated that the clay mineral layers acted as a protective barrier and improved the flame retardant of the nanocomposites.

Table III presented the results of element analysis for PMMA/OMMT, PMMA-DPEAA10, and PMMA-DPEAA/OMMT after cone calorimeter tests. As shown in Table III, around 24% phosphorus and 22% carbon still remained in the chars of PMMA-DPEAA10, indicating the excellent carbonization of DPEAA. The carbon content of the char for PMMA-DPEAA/OMMT was higher than that of PMMA/OMMT and PMMA-DPEAA10, which indicated that the synergistic effect of DPEAA and montmorillonite improved char-forming ability of the nanocomposites.

TABLE II
Cone Calorimetry Data for Various Samples at 35 kW/m^2

Sample	t_{ign} (s)	PHRR (kW/m^2)	THR (MJ/m^2)	ASEA (m^2/kg)	AMLR (g/s)
PMMA	26 ± 2	496 ± 11	67 ± 0.8	616 ± 16	0.079 ± 0.007
PMMA/OMMT	31 ± 2	395 ± 8	65 ± 0.9	602 ± 18	0.068 ± 0.005
PMMA-DPEAA5	37 ± 3	387 ± 7	59 ± 0.7	512 ± 15	0.064 ± 0.006
PMMA-DPEAA10	42 ± 3	367 ± 6	57 ± 0.7	353 ± 15	0.063 ± 0.005
PMMA-DPEAA/OMMT	48 ± 2	295 ± 8	54 ± 0.6	336 ± 16	0.056 ± 0.004

t_{ign}, time of ignition; PHRR, peak release rate; THR, total heat release; ASEA, average-specific extinction area; AMLR, average mass loss rate.

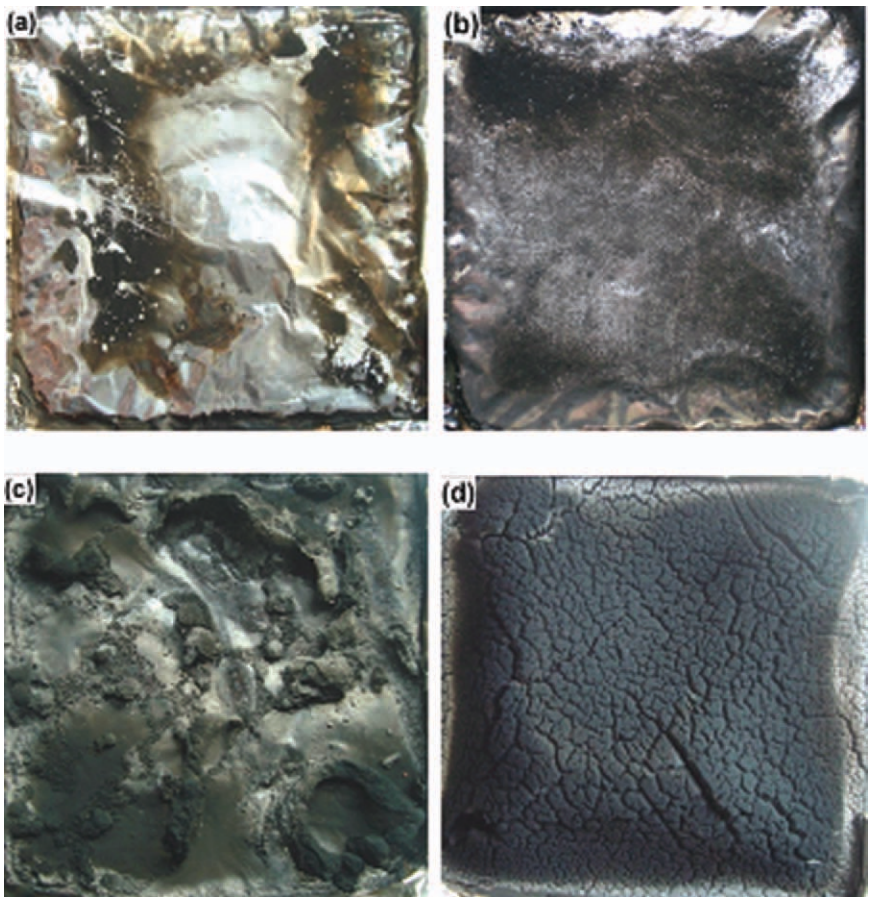

Figure 8 Digital photos of the residues after cone calorimeter testing: (a) PMMA, (b) PMMA/OMMT, (c) PMMA-DPEAA10, and (d) PMMA-DPEAA/OMMT. [Color figure can be viewed in the online issue, which is available at wileyonlinelibrary.com.]

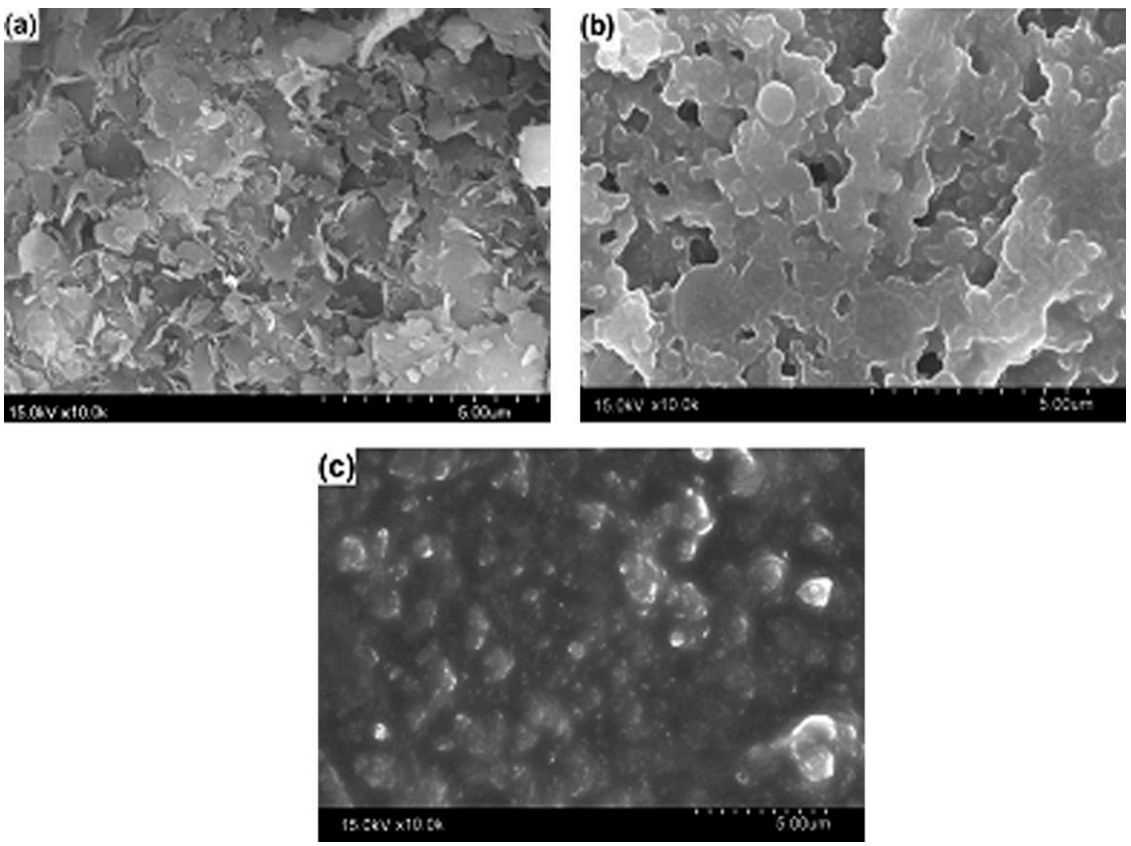

Figure 9 SEM images of the char after cone calorimeter testing: (a) PMMA/OMMT, (b) PMMA-DPEAA10, and (c) PMMA-DPEAA/OMMT.

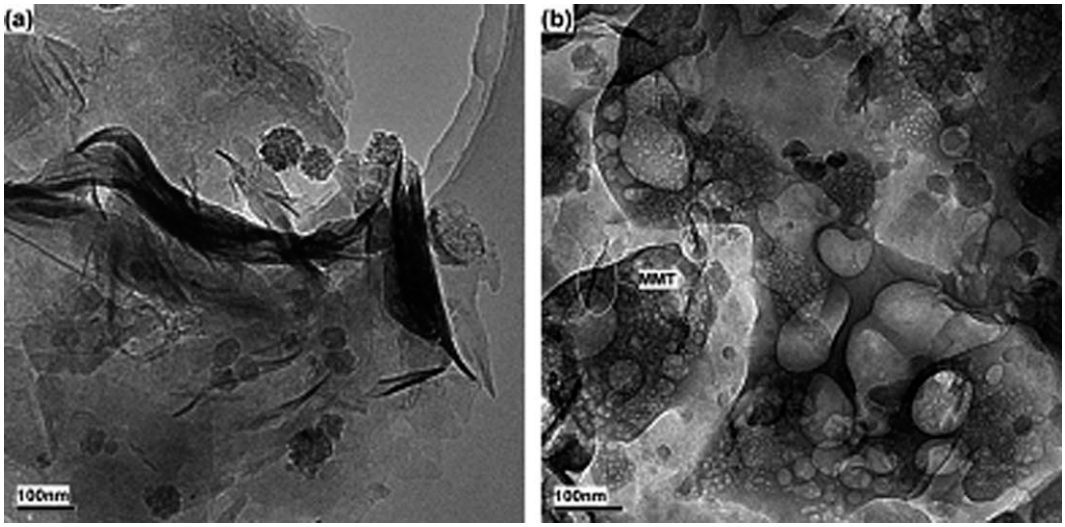

Figure 10 TEM images of the char after cone calorimeter testing: (a) PMMA/OMMT and (b) PMMA-DPEAA/OMMT.

TABLE III
The Results of EDX Analysis of the Residues After Cone Calorimeter Testing

Sample	Mass content (wt %)					
	C	O	P	Si	Al	Mg
PMMA/OMMT	7.98 ± 0.13	54.47 ± 0.88	–	25.82 ± 0.03	9.46 ± 0.17	2.27 ± 0.08
PMMA-DPEAA10	22.25 ± 0.42	53.25 ± 0.86	24.50 ± 0.14	–	–	–
PMMA-DPEAA/OMMT	28.86 ± 0.14	41.51 ± 0.80	14.49 ± 0.13	10.64 ± 0.20	3.66 ± 0.09	0.84 ± 0.04

Mechanical properties

Table IV showed that the data for the mechanical properties of PMMA and its nanocomposites. Compared with pure PMMA, PMMA/OMMT composites filled with 5 wt % showed a 15% increase in tensile strength to 21.4 MPa, a 12% increase in elastic modulus to 288.3 MPa, little change in elongation at break, which indicated the strength effect of OMMT for PMMA matrix. Tensile tests on PMMA-DPEAA5 and PMMA-DPEAA10 showed marked reduction of in the tensile strength and elastic modulus compared with pure PMMA. Fortunately, after adding OMMT into PMMA-DPEAA copolymer, the mechanical properties, including tensile strength and elastic modulus, were to some extent improved compared with PMMA-DPEAA10. Meanwhile, the mechanical properties of PMMA-DPEAA/OMMT nanocomposites exhibited almost no deterioration compared with pure PMMA.

TABLE IV
Mechanical Properties of PMMA and Its Nanocomposites

Sample	Tensile strength (MPa)	Elastic modulus (MPa)	Elongation at break (%)
PMMA	18.65	256.4	59.6
PMMA/OMMT	21.44	288.3	44.9
PMMA-DPEAA5	17.43	247.8	78.9
PMMA-DPEAA10	16.15	232.7	89.7
PMMA-DPEAA/OMMT	18.03	259.6	51.74

CONCLUSIONS

The reactive phosphorus–nitrogen-containing monomer, DPEAA, was synthesize and characterized. PMMA-DPEAA/OMMT nanocomposites were prepared by *in situ* polymerization by incorporating MMA, DPEAA, and OMMT. The results from XRD and TEM showed that exfoliated PMMA-DPEAA/OMMT nanocomposites were formed. A synergistic effect was found between DPEAA and montmorillonite which improved the thermal stability and flame retardancy of PMMA. Compared with pure PMMA, the PHRR of PMMA-DPEAA/OMMT was reduced by about 40%. The LOI value of PMMA-DPEAA/OMMT reached 27.3%. The SEM and TEM images confirmed that a compact, dense, and uniform intumescent char was formed for PMMA-DPEAA/OMMT nanocomposites after combustion. The EDX analysis results indicated that the carbon content of the char for PMMA-DPEAA/OMMT increased by the synergistic effect of DPEAA and montmorillonite.

References

1. Wang, D.-Y.; Wang, Y.-Z.; Wang, J.-S.; Chen, D.-Q.; Zhou, Q.; Yang, B.; Li, W.-Y. Polym Degrad Stab 2005, 87, 171.
2. Ge, X.-G.; Wang, D.-Y.; Wang, C.; Qu, M.-H.; Wang, J.-S.; Zhao, C.-S.; Jing, X.-K.; Wang, Y.-Z. Euro Polym J 2007, 43, 2882.
3. Wang, T.-Z.; Chen, K.-N. J Appl Polym Sci 1999, 74, 2499.
4. Chen, G.-H.; Yang, B.; Wang, Y.-Z. J Appl Polym Sci 2006, 102, 4978.
5. Ai, H.; Xu, K.; Liu, H.-A.; Chen, M.-C. Polym Eng Sci 2009 49, 1879.
6. Gao, L.-P.; Wang, D.-Y.; Wang, Y.-Z.; Wang, J.-S.; Yang, B. Polym Degrad Stab 2008, 93, 1308.
7. Lu, Z.; Cheng, B.; Huang, X.; Ren, Y.; Yan, G.; Xi, P.; Li, Z.; Zhang, J.; Kang, W. Patent (CN) 101113211, 2008.
8. Paula, D. R.; Robeson, L. M. Polymer 2008, 49, 3187.
9. Rao, Y.-Q.; Pochan, J. M. Macromolecules 2007, 40, 290.
10. Shi, Y.-R.; Kashiwagi, T.; Walters, R. N.; Gilman, J. W.; Lyon, R. E.; Sogah, D. Y. Polymer 2009, 50, 3478.
11. Vyazovkin, S.; Dranca, I.; Fan, X.-W.; Advincula, R. J Phys Chem B 2004, 108, 11672.
12. Joseph, S.; Focke, W. W. Polym Compos 2011, 32, 252.
13. Lakshmi, M. S.; Narmadha, B.; Reddy, B. S. R. Polym Degrad Stab 2008, 93, 201.
14. Han, Y. Q. Polym Compos 2009, 30, 66.
15. Lim, S. K.; Kim, J. W.; Chi, I. N.; Kwon, Y. K.; Choi, H. J. Chem Mater 2002, 14, 1989.
16. Rehab, A.; Akelah, A.; Agag, T.; Shalaby, N. Polym Compos 2008, 28, 108.
17. Chuang, T.-H.; Guo, W.-J.; Cheng, K.-C.; Chen, S.-W.; Wang, H.-T.; Yen, Y.-Y. J Polym Res 2004, 11, 169.
18. Asif, A.; Lakshmana Rao, V.; Saseendran, V.; Ninan, K. N. Polym Eng Sci 2009, 49, 756.
19. Song, R.-J.; Wang, Z.; Meng, X.-Y., Zhang, B.-Y.; Tang, T. J Appl Polym Sci 2007, 106, 3488.
20. Tang, Y.; Hu, Y.; Wang, S.-F.; Gui, Z.; Chen, Z.-Y.; Fan, W.-C. Polym Int 2003, 52, 1396.
21. Gilman, J. W.; Jackson, C. L.; Morgan, A. B.; Harris, R., Jr. Chem Mater 2000, 12, 1866.
22. Berta, M.; Lindsay, C.; Pans, G.; Camino, G. Polym Degrad Stab 2006, 91, 1179.
23. Bourbigot, S.; Devaux, E.; Xavier Polym Degrad Stab 2002, 75, 397.
24. Zhang, H.-F.; Wang, Y.-Q.; Wu, Y.-P.; Zhang, L.-Q.; Yang, J. J Appl Polym Sci 2005, 97, 844.
25. Ma, H.-Y.; Xu, Z.-B.; Tong, L.-F.; Gu, A.-G.; Fang, Z.-P. Polym Degrad Stab 2006, 91, 2951.
26. Valera-Zaragoza, M.; Ramírez-Vargas, E.; Medellín-Rodríguez, F. J.; Huerta-Martínez, B. M. Polym Degrad Stab 2006, 91, 1319.
27. Xie, F.; Wang, Y.-Z.; Yang, B.; Liu, Y. Macromol Mater Eng 2006, 291, 247.
28. Ma, Z.-L.; Gao, J.-G.; Bai, L.-G. J Appl Polym Sci 2004, 92, 1388.
29. Wang, D.-Y.; Cai, X.-X.; Qu, M.-H.; Liu, Y.; Wang, J.-S.; Wang, Y.-Z. Polym Degrad Stab 2008, 93, 2186.
30. Peng, H.-Q.; Zhou, Q.; Wang, D.-Y.; Chen, L.; Wang, Y.-Z. J Ind Eng Chem 2008, 14, 589.
31. Isitman, N.-A.; Kaynak, C. Polym Degrad Stab 2010, 95, 1523.
32. Costache, M.-C.; Wang, D.-Y; Heidecker, M.-J.; Manias, E.; Wilkie, C.-A. Polym Adv Tech 2006, 17, 272.
33. Zhu, J.; Start, P.; Mauritz, K.-A.; Wilkie, C.-A. Polym Degrad Stab 2002, 77, 253.
34. Tang, Y.; Wang, D.-Y.; Jing, X.-K.; Ge, X.-G.; Yang, B.; Wang, Y.-Z. J Appl Polym Sci 2008, 108, 1216.
35. Huang, G.-B.; Gao, J.-R.; Li, Y.-J.; Han, L. Wang; X. Polym Degrad Stab 2010, 95, 245.
36. Isitman, N.-A.; Gunduz, H.-O.; Kaynak, C. Polym Degrad Stab 2009, 94, 2241.
37. Ma, H.-Y.; Tong, L.-F.; Xu, Z.-B.; Fang, Z.-P. Appl Clay Sci 2008, 42, 238.